Islamic Azad University

Journal of

Optoelectronical Nanostructures

Winter 2025 / Vol. 10, No. 4

Research Paper (Pape Type)

High-Performance Dual-Wavelength All-Optical Reflective Semiconductor Optical Amplifier Utilizing Solution-Processed Quantum Dots

Hamed Ghatei [1], Samiye Matloub *[,1], Hamed Baghban [2]

[1] Quantum and Photonic Research Lab., Faculty of Electrical and Computer Engineering, University of Tabriz, Tabriz, Iran

[2] Faculty of Electrical and Computer Engineering, University of Tabriz, Tabriz, Iran

Received:
Revised:
Accepted:
Published:

Use your device to scan and read the article online

DOI: https://doi.org/10.71577/jopn.2025.1197497

Keywords:
Dual-wavelength, Quantum dot Reflective Semiconductor Optical Amplifier

Abstract

This study presents a dual-wavelength all-optical quantum dot reflective semiconductor optical amplifier (QD-RSOA) designed for modern optical communication systems. Using solution-processed InAs/AlAs quantum dots, the device operates at 1.31 μm and 1.55 μm, allowing simultaneous or independent signal amplification. Unlike conventional amplifiers, it relies on optical pumping instead of electrical injection, improving gain recovery speed and efficiency. The reflective design enhances carrier replenishment, leading to better modulation depth, broader gain bandwidth, and superior spectral response. Its dual-wavelength capability makes it ideal for applications like wavelength-division multiplexing (WDM) and all-optical signal processing. Numerical simulations confirm its superior gain performance and stability over traditional QD-SOAs. This advancement supports high-speed, multi-channel optical networks, meeting the increasing demand for efficient photonic communication systems.

Citation: Hamed Ghatei Khiabani Azar , Samiye Matloub , Hamed Baghban . High-Performance Dual-Wavelength All-Optical Reflective Semiconductor Optical Amplifier Utilizing Solution-Processed Quantum Dots. **Journal of Optoelectronical Nanostructures.** 2025; 1 (1): 48-58

***Corresponding author: Samiye Matloub**
Address: Quantum and Photonic Research Lab., Faculty of Electrical and Computer Engineering, University of Tabriz, Tabriz, Iran.
Tell: 009891106397 **Email:** matloub@tabrizu.ac.ir

(QD-RSOA), Gain recovery. Optical pumping, Solution-processed QDs.

1. INTRODUCTION

In recent years, with the tremendous growth of computer and communication systems, the need to develop devices capable of transferring data faster and more efficiently has already been felt, and with the emergence of telecommunications and optical networks as a new communication platform, only small part of it has been met. To address this challenge, it is imperative to enhance the operating bandwidth of optical components to meet the growing demands of advanced photonic systems. Among the various technologies available, quantum dot semiconductor optical amplifiers (QD-SOAs) have garnered considerable interest due to their remarkable versatility and wide-ranging applications in photonics. These devices play a pivotal role in facilitating high-bit-rate optical switching, which is essential for modern communication networks.

The Quantum Dot Semiconductor Optical Amplifier (QD-SOA) structure has demonstrated exceptional performance when utilized in a Passively Integrated Quantum Source (PIQS), particularly due to its impressive saturated gain. At an operating wavelength of 1.55 μm, the polarization sensitivity remains remarkably low, measuring less than 0.1 dB for thicknesses up to 1.7 μm. Even as the thickness increases beyond this point, the polarization sensitivity remains well-controlled, staying below 1 dB. This indicates the robustness of the QD-SOA structure in maintaining stable optical properties, making it a promising candidate for applications requiring high efficiency and minimal polarization dependence [1-3].

Additionally, QD-SOAs are instrumental in enabling wavelength-division multiplexing, a critical technology for maximizing data transmission capacity in fiber-optic communication systems. Their ability to support all-optical signal processing further underscores their importance, as they help eliminate the need for electronic conversions, thereby enhancing system speed and efficiency. These characteristics position QD-SOAs as a cornerstone technology for advancing photonic applications, as highlighted in [4-7]. Due to their distinctive characteristics, these components play a crucial role in overcoming the inherent limitations associated with traditional optical devices. By effectively addressing these constraints, they contribute significantly to the advancement of modern optical technologies, ultimately facilitating the development of next-generation optical communication systems. Their ability to enhance performance, improve efficiency, and ensure greater reliability makes them indispensable for future

high-speed and high-capacity communication networks.

Quantum dot semiconductor optical amplifiers (QD-SOAs) stand out due to their remarkable characteristics, which confer significant advantages in various applications. Pivotal features include their exceptionally fast gain recovery times, as demonstrated in studies [7,8], enabling swift response and efficient operation. Additionally, they exhibit high saturation power, as detailed in [9], which supports robust performance even under demanding conditions. Unlike traditional approaches, QD-SOAs offer patterning-free optical amplification, as highlighted in [10], simplifying implementation while maintaining effectiveness. Furthermore, their outstanding performance speed, emphasized in [11], positions them as a leading choice for next-generation optical systems. Collectively, these features underline the transformative potential of QD-SOAs, as discussed comprehensively in [12]. The presence of a gap between the QD levels and the wetting layer (WL) makes QD-SOAs more favorable candidate compared to bulk and quantum well SOAs. In fact, QD-SOAs have been shown to have lower noise Fig. and higher output power than bulk and quantum well amplifiers in comparative studies [13,14]. Additionally, due to their smaller cross sections in carrier-photon interactions, QD-SOAs exhibit interesting characteristics like lower saturation power, reduced frequency noises, and shorter carrier relaxation lifetimes. These characteristics, combined with a reflective end facet [15], make quantum dot reflective semiconductor optical amplifiers (QD-RSOAs) as a promising option for high-speed data amplifiers in colorless WDM-PONs [16,17], surpassing the bandwidth limitations of SOAs [18]. It is essential for electronic devices connected to QD-SOAs to ensure robust protection against various risks such as electromagnetic interference, source instability, and other potential threats to the system's integrity [19]. These factors can undermine the performance and reliability of the device, making it crucial to prioritize safety measures that mitigate such risks.

In comparative studies, one significant difference between traveling-wave SOAs and RSOAs lies in their operational principle. Unlike traveling-wave SOAs, RSOAs function based on a double-pass mechanism, which requires a more sophisticated modeling approach. This is necessary to account for the effects of transit time and the interactions between counter-propagating pulses on the dynamics of carriers and gain. The double-pass operation leads to complex interactions, where the reflected pulses overlap and influence the spatial distribution of photons and carrier densities, creating significant pattern effects.

Because of these intricate interactions, traditional numerical models used for QD-SOAs, which typically focus on single-pass configurations, may not be sufficient or accurate for determining the collision times of counter-propagating pulse streams in RSOAs. The interactions between these counter-propagating pulses can introduce additional complexities that are not captured by standard models [20-25]. Therefore, more advanced modeling techniques are required to effectively simulate and understand the behavior of RSOAs, ensuring their performance is accurately predicted and optimized for practical applications.

One of the primary challenges in optimizing the performance of quantum-dot reflective semiconductor optical amplifiers (QD-RSOAs) is maintaining uniform electrode surfaces along the waveguide. Small fluctuations in optical intensity lead to variations in carrier concentration throughout the device length, which adversely affects efficiency and reliability. Various complex methods have been proposed to modify injection currents to address this issue, but these approaches often fall short due to the intricacy and expense associated with achieving perfectly uniform current injection.

An innovative and promising approach to overcoming the limitations of traditional methods involves substituting electrical signals with optical signals. This shift effectively removes the necessity for a carrier transport layer, leading to several key advantages. By implementing an optical pumping technique, the overall complexity of the device fabrication process is significantly reduced, making manufacturing more efficient and cost-effective. Additionally, this method helps minimize optical losses, thereby improving signal integrity and boosting overall system performance. Furthermore, the operational frequency of Quantum Dot Reflective Semiconductor Optical Amplifiers (QD-RSOAs) is notably enhanced, allowing for faster and more efficient optical signal processing. These benefits, as highlighted in [26,49], underscore the potential of optical pumping as a transformative technique in advancing next-generation optical communication technologies.By removing the reliance on electrical injection, the optical pumping approach offers a more straightforward and effective means to optimize device performance.

QD-RSOAs are particularly well-suited for cost-sensitive applications, such as implementing passive optical networks (PONs), where affordability and efficiency are critical. These amplifiers provide a practical and economical solution for meeting the stringent demands of PONs, as highlighted in [27,28]. Furthermore, the growing demand for high-speed optical communication networks has driven the need to overcome the inherent limitations of electronic signal processing. This has spurred interest in all-optical signal processing

methods, where QD-RSOAs play a pivotal role in addressing these challenges and supporting the development of next-generation optical networks.

Given the superiority of QD-RSOA with optical pump, the goal is to realize this amplifier in a two-channel configuration using special techniques. With this modification, we can achieve the nature and advantages of a dual-channel amplifier along with the advantages mentioned above. That is, each channel will be able to amplify the input signal both separately and simultaneously. In this paper, a novel concept of a two-channel QD all-optical amplifier is introduced. The innovative device is conceived to be synthesized through the solution-processed InAs/AlAs QD core/shell structure, which provides higher absorption, high efficiency, low-cost fabricating, room-temperature processing, ease of large-area fabrication, and high tunability. Distinguishing itself from conventional approaches, our novel two-channel QD-RSOA provides a unique capability: adjustability to amplify selective wavelengths through the careful tuning of QDs' sizes. The high-speed two-channel quantum dot semiconductor optical amplifier (QD-SOA) operating in reflective mode, equipped with a rapid gain recovery mechanism, demonstrates exceptional versatility and potential across a wide range of applications. These include all-optical signal processing, wavelength conversion, spectroscopy, laser gyroscopes, and the design of logic gates. The enhanced performance of this device, particularly its superior operational speed and improved gain recovery process compared to traditional QD-SOAs, sets it apart as a cutting-edge solution in optical technology.

One of its key advantages is the ability to eliminate the reliance on electrical components within optical amplifiers, transitioning to a fully optical framework. This fundamental shift paves the way for seamless integration with other optical devices, fostering advancements in compact and efficient photonic systems. This capability aligns with the increasing demand for high-speed, low-latency optical communication and processing technologies, as highlighted in [29-36].

Moreover, the reflective mode of operation enhances its compatibility with modern optical systems, enabling more compact architectures and reducing complexity. This makes the high-speed two-channel QD-SOA not only a high-performance solution but also a cost-effective and scalable option for next-generation optical networks and instrumentation. Its broad applicability underscores its value in addressing the evolving challenges of high-speed optical communication and precision measurement systems.

This research provides a comprehensive analysis of Quantum Dot Semiconductor Optical Amplifiers (QD-SOAs) configured in a reflective mode, with a particular focus on amplification driven by optical pumping across two

distinct wavelength channels. Notably, this is the first study to explore this approach in detail. To demonstrate the effectiveness of optical pumping, a comparative evaluation is conducted between a traditionally used electrically pumped Quantum Dot Reflective Semiconductor Optical Amplifier (QD-RSOA) and the proposed optically pumped QD-RSOA. This comparison highlights the superior advantages of optical pumping, particularly in terms of accelerating the gain recovery process and enhancing overall operational speed. The findings underscore the potential of optical pumping as a key technique for improving the performance and efficiency of next-generation optical communication systems. Unlike traditional quantum dot reflective semiconductor optical amplifiers (QD-RSOAs) that rely on electrical pumping, this advanced device employs an optical pumping mechanism to transfer carriers from the valence band (VB) to the corresponding conduction band (CB). This optical pumping approach not only simplifies the architecture but also facilitates the seamless integration of the pump source with the amplifier on a single chip. Such integration leads to significant improvements in gain recovery dynamics and enables faster operational speeds, enhancing the overall performance of the device, as supported by [37, 38].

The research and advancement of a two-channel amplifier, along with the exploration of an all-optical amplifier, are driven by the goal of developing a high-performance device that meets both technical and commercial demands. The primary motivation behind this endeavor is to design an amplifier that not only enhances operational efficiency but also aligns with industry standards for cost-effectiveness and scalability. By optimizing performance while minimizing complexity, these innovations aim to pave the way for more practical and widely adoptable solutions in modern optical communication systems. Optical pumping, in particular, eliminates the need for complex electrical injection systems, reducing manufacturing costs while simultaneously addressing performance bottlenecks. By focusing on all-optical designs, this approach ensures greater compatibility with modern photonic systems, where speed and efficiency are paramount.

Moreover, the simplified design brought about by optical pumping makes it easier to scale the technology for mass production, meeting the demands of high-speed optical communication networks. This innovation underscores the pursuit of practical and economically sustainable solutions in the field of photonics, with the potential to revolutionize the performance and affordability of next-generation amplifiers.

2. CONCEPT AND MODELING

Our study presents an innovative approach that employs two distinct sizes of core/shell synthesized quantum dots (QDs) to develop a high-speed, dual-channel, all-optical QD-RSOA. This method offers significant advantages in terms of cost-efficiency and simplicity in the synthesis of QDs. Additionally, the radii of the quantum dots can be precisely adjusted to align with specific accuracy requirements and applications, enhancing their versatility and performance.

The proposed all-optical QD-RSOA operates effectively at dual wavelengths of 1.31 μm and 1.55 μm, which are commonly used in optical communication systems, and is built on a glass substrate. Fig. 1(a) illustrates the device configuration, where pump and probe signals are transmitted through separate channels, ensuring minimal interference and optimal performance. This dual-channel design is particularly advantageous for applications requiring simultaneous processing of signals at different wavelengths, making it a promising solution for advanced photonics and optical communication technologies. By combining innovative quantum dot synthesis with practical design, this approach pushes the boundaries of high-speed optical amplification and broadens the potential for integration into cost-sensitive and high-performance systems.

The core is made up of InAs, while the shell consists of AlAs, forming the absorber layer crucial to the proposed structure through solution process technology. It is important to note that the QDs can be distinguished by their radii, with R1 and R2 representing channel-1 and channel-2, respectively. Traditionally, carrier injection via electrical pumping involves layers for electron and hole transfer alongside the active layer and substrate. Our approach differs by exclusively utilizing colloidal QDs within the active layer. This unique setup allows for effective light confinement within the active region as the refractive index of the active layer surpasses that of the transmission layers. Instead of transmission layers, we opt to use an optical pump for carrier population inversion. The design of our device incorporates a carefully optimized active region strategically positioned between regions of air and glass. These materials are selected for their low refractive indices, which play a crucial role in enhancing light confinement within the active region, thereby improving the device's optical efficiency. This configuration ensures that light remains concentrated where it is most effectively amplified, supporting superior device performance.

Within the active region, indium arsenide (InAs) quantum dots (QDs) of

varying sizes are embedded to target specific wavelengths for dual-channel operation. Quantum dots with a radius of 3.75 nm are tailored for channel-1, operating at a wavelength of 1.55 μm, while smaller quantum dots with a radius of 3 nm are optimized for channel-2 at 1.31 μm. These QDs are housed within an aluminum arsenide (AlAs) cladding layer, which serves multiple functions, including providing structural stability and optimizing the refractive index contrast to further enhance light confinement.

To preserve the waveguide properties essential for efficient signal transmission, an additional AlAs layer is strategically placed over the active region. This layer ensures that the guided light remains confined within the desired optical path, minimizing losses and maintaining high operational efficiency. The overall design reflects a meticulous balance between material selection and structural configuration, enabling effective wavelength-specific amplification and paving the way for advanced applications in optical communication and signal processing.

In this context, a novel superimposed solution-processed QD-RSOA model is proposed for an InAs/AlAs structure, where two types of quantum dots (QDs) are classified based on their size distribution. This approach aims to enhance wideband optical gain by combining QDs with varying sizes, thereby tailoring the optical gain to achieve specific bandwidths and gain levels. The concept involves the superimposition of quantum dots to engineer an optical gain response across a broad spectrum.

In the proposed model, continuous wave (CW) signals are employed as the pump source, operating at wavelengths of 866 nm for channel-1 and 683 nm for channel-2. Meanwhile, a Gaussian pulse is used as the probe signal, with wavelengths of 1.55 μm for channel-1 and 1.31 μm for channel-2. This setup allows for effective dual-wavelength operation, enabling efficient signal amplification across both channels.

To ensure a fair comparison between the performance of QD-SOAs and QD-RSOAs, both devices are constructed using the same material composition and structural parameters. The key difference lies in the rear facet reflectivity (R) configuration, which is set to 0 for the QD-SOA, while a mirror is placed at the rear facet of the QD-RSOA to create a double-pass mechanism for the traveling signals. This modification in the QD-RSOA design enhances the efficiency of the device by allowing the signal to pass through the structure twice, ultimately improving gain and overall performance. This comparative analysis highlights the advantages of the QD-RSOA architecture in terms of efficiency and performance.

The structural parameters are specifically designed for QD radii, with R1 set at 3.75 nm and R2 set at 3 nm. When the pump signal is applied, electrons absorb energy from the excited state of the valence band (ESv) to the excited state of the conduction band (ESc) and then quickly transition to the ground state of the conduction band (GSc) due to a short relaxation time. The CW pump signal is utilized to transfer electrons from the ESv to the ESc. As the ESv depletes, electrons from the GSv quickly decay into the ESv, ensuring that the GSv remains empty. Additionally, the pump signal continuously transfers electrons from the ESv to the ESc, leading to a rapid decay of electrons from the ESc to the GSc, keeping it consistently full of electrons.

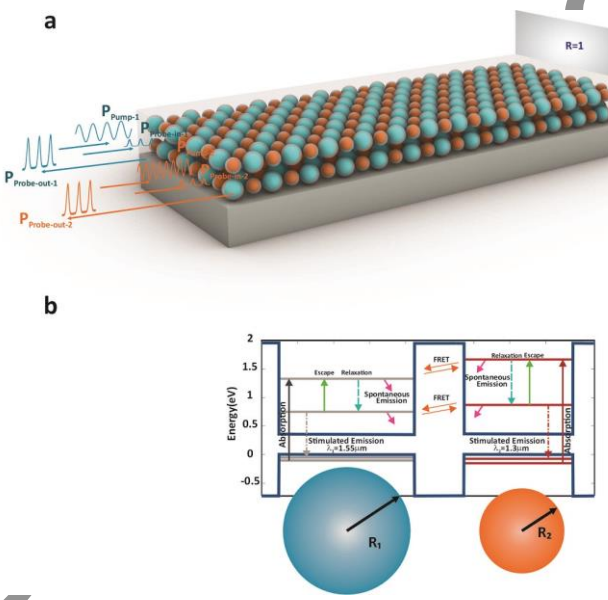

Fig. 1. presents a schematic representation of the proposed two-channel All-Optical Quantum Dot Reflective Semiconductor Optical Amplifier (QD-RSOA), highlighting its structural and functional aspects. (a) Shows an array arrangement featuring Quantum Dots (QDs) of two different sizes embedded within a core/shell InAs/AlAs structure, demonstrating their spatial distribution. (b) Illustrates the energy band diagram of the proposed design, depicting key carrier dynamics such as absorption, emission, recombination, relaxation, and escape processes. Additionally, it highlights the occurrence of Förster Resonance Energy Transfer (FRET) between the two differently sized QDs, which plays a significant role in energy transfer efficiency.

Essentially, the purpose of the pump signal is to maintain the GSc filled with electrons while keeping the GSv devoid of electrons, creating population inversion. When a photon with a wavelength of 1.55 μm enters this system, equal to the difference between the GSc and GSv, it triggers stimulated emission rather than absorption due to the population inversion. This results in the generation of photons equivalent to the number of electrons at the GSc level. Therefore, a single photon can yield a multitude of photons, essentially amplifying the input probe signal at 1.55 μm. Stimulated emission ensures that the produced photons have the same frequency and phase as the input signal. To prevent nonlinearity in the system and maintain gain, it is essential to keep the amplitude of the input probe signal low. In QD-SOAs, the output signal is obtained from the end of the structure, whereas in QD-RSOAs, the end is reflected and the wave passes through the active area twice and is obtained from the front facet. It is anticipated that the gain in QD-RSOAs will be approximately double of that for QD-SOAs with the same active area length, in addition to other benefits provided by this structure.

It is crucial to note that the solution process, whose versatility extends to diverse optoelectronics and photonics engineering devices, has the potential for commercializing industrial products. Chemical synthesis methods are exploited to customize the size of the QDs through engineering various parameters such as concentration, temperature, etc [38-44]. Colloidal QDs typically range in diameter from 1 nm to 10 nm, with deviations in size of 0.1 nm achievable under suitable experimental conditions [45-49]. Although procedures for fabricating QDs are accurate enough, slight variations in size of these QDs can yield in different properties. The size variation of QDs can lead to inhomogeneous broadening (IHB), causing energy level distribution. The inhomogeneous broadening of energy levels is modeled using a Gaussian function to account for the non-uniformity in QDs size and their impact on absorption spectra. To align with experimental data for QD-SOAs and achieve realistic values for QD-RSOAs, coupling losses of 3-dB per facet are taken into account. Due to differences in the sizes of quantum dots (QDs), there is an inhomogeneous broadening (IHB) of the confined energy levels within the QD ensemble. To account for this variation, the ensemble is categorized into 2M+1 distinct groups, where each group consists of QDs that share identical energy levels. The energy separation between adjacent groups is set at ΔE=1 meV. This classification helps in analyzing the energy distribution of the QDs more effectively. A visual representation of the energy band structure, along with the specific energy positions of the accumulated QDs, is provided in Fig. 1(b),

illustrating how these discrete energy levels are arranged.

When developing a model for the experimental setup, it is crucial to consider the impact of the Fluorescence or Förster Resonance Energy Transfer (FRET) phenomenon. FRET takes place when two quantum dots (QDs) of different sizes are positioned in close proximity, facilitating the transfer of energy or carriers between them. This interaction plays a significant role in the dynamics of the system and must be accounted for to ensure the accuracy of the model [50,51].

To incorporate the FRET phenomenon, a set of rate equations is established for four energy levels, specifically the ground state (GS) and excited state (ES) in both the conduction and valence bands. These equations are modified to include the Förster process, introducing two additional pathways for carrier dynamics. This adjustment ensures that the energy transfer effects between the QDs are accurately represented.

In addition to these structural modifications, the proposed model incorporates a set of equations that govern the transmission of optical signals for both the probe and pump. These equations are formulated based on two fundamental assumptions to ensure accurate modeling and simulation.

The first assumption posits that light waves travel through the structure exclusively along the z-direction, with computational steps progressing incrementally from 0 to L. This approach simplifies the mathematical treatment of light-matter interactions within the system, enabling a more straightforward analysis of how optical signals propagate through the medium. The second assumption is that the time intervals used in solving these equations are extremely small. By adopting such fine temporal resolution, the model can precisely capture rapid dynamic variations in both carrier behavior and optical signal characteristics, ensuring a more detailed and accurate representation of the amplification and energy transfer processes.

By integrating these factors, including the FRET phenomenon and the associated rate equations, the model provides a comprehensive framework for understanding the energy transfer dynamics and optical signal processing in the experimental setup. This enhances the accuracy and predictive power of the simulation, contributing to the development of more effective quantum dot-based optical devices.

3. The Developed Rate And Propagation Equations

The operational efficiency of the developed two-channel QD-RSOA is mainly influenced by the interactions between carriers and photons. Although the semiconductor Bloch equation provides a more accurate way to study and

simulate these behaviors, its computational demands and time-consuming nature have led to the use of rate and propagation equations, which have produced positive outcomes. The transmission of CW pump signals and square-pulse train probe signals is done in the z-direction. The sophisticated coupled rate and propagation equations for the suggested configuration, utilizing the parameters detailed in [26].

$$\frac{dn^c_{g_{n,1}}(z,t)}{dt} = \frac{n^c_{g_{n,1}}(z,t)}{\tau_{down\_trans\_g}}\left(1-f^c_{g_{n,2}}(z,t)\right)+\frac{n^c_{g_{n,2}}(z,t)}{\tau_{up\_trans\_g}}\left(1-f^c_{g_{n,1}}(z,t)\right) - \frac{n^c_{g_{n,1}}(z,t)}{\tau_{gr}}\left(1-f^v_{g_{n,1}}(z,t)\right)+\frac{n^c_{e_{n,1}}(z,t)}{\tau^c_{eg}}\left(1-f^c_{g_{n,1}}(z,t)\right) - \frac{n^c_{g_{n,1}}(z,t)}{\tau^c_{ge}}\left(1-f^c_{e_{n,1}}(z,t)\right) - \sum_{m=1}^{2M+1}\Gamma Lg_{m,n,1}\frac{\left(P^{Probe,+}_{m,1}+P^{Probe,-}_{m,1}\right)}{E^{Probe}_{m,1}}\left(f^c_{g_{m,1}}(z,t)-f^v_{g_{m,1}}(z,t)\right) \quad (1)$$

$$\frac{dn^c_{g_{n,2}}(z,t)}{dt} = \frac{n^c_{g_{n,1}}(z,t)}{\tau_{down\_trans\_g}}\left(1-f^c_{g_{n,2}}(z,t)\right)-\frac{n^c_{g_{n,2}}(z,t)}{\tau_{up\_trans\_g}}\left(1-f^c_{g_{n,1}}(z,t)\right) - \frac{n^c_{g_{n,2}}(z,t)}{\tau_{gr}}\left(1-f^v_{g_{n,2}}(z,t)\right)+\frac{n^c_{e_{n,2}}(z,t)}{\tau^c_{eg}}\left(1-f^c_{g_{n,2}}(z,t)\right) - \frac{n^c_{g_{n,2}}(z,t)}{\tau^c_{ge}}\left(1-f^v_{e_{n,2}}(z,t)\right) - \sum_{m=1}^{2M+1}\Gamma Lg_{m,n,2}\frac{\left(P^{Probe,+}_{m,2}+P^{Probe,-}_{m,2}\right)}{E^{Probe}_{m,2}}\left(f^c_{g_{m,2}}(z,t)-f^v_{g_{m,2}}(z,t)\right) \quad (2)$$

$$\frac{dn^c_{e_{n,1}}(z,t)}{dt} = -\frac{n^c_{e_{n,1}}(z,t)}{\tau_{down_{trans_e}}}\left(1-f^c_{e_{n,2}}(z,t)\right)+\frac{n^c_{e_{n,2}}(z,t)}{\tau_{down_{trans_e}}}\left(1-f^c_{e_{n,1}}(z,t)\right) - \frac{n^c_{e_{n,1}}(z,t)}{\tau_{er}}\left(1-f^v_{e_{n,1}}(z,t)\right)+\frac{n^c_{g_{n,1}}(z,t)}{\tau^c_{ge}}\left(1-f^c_{e_{n,1}}(z,t)\right) - \frac{n^c_{e_{n,1}}(z,t)}{\tau^c_{eg}}\left(1-f^c_{g_{n,2}}(z,t)\right) + \sum_{m=1}^{2M+1}\Gamma L\alpha_{m,n,1}\frac{\left(P^{Pump,+}_{m,1}+P^{Pump,-}_{m,1}\right)}{E^{Pump}_{m,1}}\left(f^v_{e_{m,1}}(z,t)-f^c_{e_{m,1}}(z,t)\right) \quad (3)$$

$$\frac{dn^c_{e_{n,2}}(z,t)}{dt} = \frac{n^c_{e_{n,1}}(z,t)}{\tau_{down_{trans_e}}}\left(1-f^c_{e_{n,2}}(z,t)\right)-\frac{n^c_{e_{n,2}}(z,t)}{\tau_{down_{trans_e}}}\left(1-f^c_{e_{n,1}}(z,t)\right) - \frac{n^c_{e_{n,2}}(z,t)}{\tau_{er}}\left(1-f^v_{e_{n,2}}(z,t)\right)+\frac{n^c_{g_{n,2}}(z,t)}{\tau^c_{ge}}\left(1-f^c_{e_{n,2}}(z,t)\right) - \frac{n^c_{e_{n,2}}(z,t)}{\tau^c_{eg}}\left(1-f^c_{g_{n,2}}(z,t)\right) + \sum_{m=1}^{2M+1}\Gamma L\alpha_{m,n,2}\frac{\left(P^{Pump,+}_{m,2}+P^{Pump,-}_{m,2}\right)}{E^{Pump}_{m,2}}\left(f^v_{e_{m,2}}(z,t)-f^c_{e_{m,2}}(z,t)\right) \quad (4)$$

$$\frac{dn^{v}_{g_{n,i}}(z,t)}{dt} = \frac{n^{c}_{g_{n,i}}(z,t)}{\tau_{gr}}\left(1-f^{v}_{g_{n,i}}(z,t)\right)+\frac{n^{v}_{e_{n,i}}(z,t)}{\tau^{v}_{eg}}\left(1-f^{v}_{g_{n,i}}(z,t)\right) - \frac{n^{v}_{g_{n,i}}(z,t)}{\tau^{v}_{ge}}\left(1-f^{v}_{e_{n,i}}(z,t)\right) + \sum_{m=1}^{2M+1}\Gamma L g_{m,n,i}\frac{\left(P^{Probe,+}_{m,i}+P^{Probe,-}_{m,i}\right)}{E^{Probe}_{m,i}}\left(f^{c}_{g_{m,i}}(z,t)-f^{v}_{g_{m,i}}(z,t)\right) \quad (5)$$

$$\frac{dn^{v}_{e_{n,i}}(z,t)}{dt} = \frac{n^{c}_{e_{n,i}}(z,t)}{\tau_{er}}\left(1-f^{v}_{e_{n,i}}(z,t)\right)+\frac{n^{v}_{g_{n,i}}(z,t)}{\tau^{v}_{eg}}\left(1-f^{v}_{e_{n,i}}(z,t)\right) - \frac{n^{v}_{e_{n,i}}(z,t)}{\tau^{v}_{ge}}\left(1-f^{v}_{g_{n,i}}(z,t)\right) - \sum_{m=1}^{2M+1}\Gamma L \alpha_{m,n,i}\frac{\left(P^{Pump,+}_{m,i}+P^{Pump,-}_{m,i}\right)}{E^{Pump}_{m,i}}\left(f^{v}_{e_{m,i}}(z,t)-f^{c}_{e_{m,i}}(z,t)\right) \quad (6)$$

$$\frac{\partial P^{Pump,+}_{m,i}}{\partial z}+\frac{1}{v_g}\frac{\partial P^{Pump,+}_{m,i}}{\partial t} = -\sum_{n=1}^{2M+1}\Gamma\alpha_{m,n,i}\left[\left(f^{v}_{e_{n,i}}(z,t)-f^{c}_{e_{n,i}}(z,t)\right)-\alpha_{int}\right]P^{Pump,+}_{m,i} \quad (7)$$

$$-\frac{\partial P^{Pump,-}_{m,i}}{\partial z}+\frac{1}{v_g}\frac{\partial P^{Pump,-}_{m,i}}{\partial t} = -\sum_{n=1}^{2M+1}\Gamma\alpha_{m,n,i}\left[\left(f^{v}_{e_{n,i}}(z,t)-f^{c}_{e_{n,i}}(z,t)\right)-\alpha_{int}\right]P^{Pump,-}_{m,i} \quad (8)$$

$$\frac{\partial P^{Probe,+}_{m,i}}{\partial z}+\frac{1}{v_g}\frac{\partial P^{Probe,+}_{m,i}}{\partial t} = +\sum_{n=1}^{2M+1}\Gamma\alpha_{m,n,i}\left[\left(f^{c}_{e_{n,i}}(z,t)-f^{v}_{e_{n,i}}(z,t)\right)-\alpha_{int}\right]P^{Probe,+}_{m,i} \quad (9)$$

$$-\frac{\partial P^{Probe,-}_{m,i}}{\partial z}+\frac{1}{v_g}\frac{\partial P^{Probe,-}_{m,i}}{\partial t} = +\sum_{n=1}^{2M+1}\Gamma\alpha_{m,n,i}\left[\left(f^{c}_{e_{n,i}}(z,t)-f^{v}_{e_{n,i}}(z,t)\right)-\alpha_{int}\right]P^{Probe,-}_{m,i} \quad (10)$$

In which the number of electrons are indicated by $n^{c}_{g_{n,i}}$, $n^{c}_{e_{n,i}}$, $n^{v}_{g_{n,i}}$, and $n^{v}_{e_{n,i}}$ in GS^c, ES^c, GS^v, and ES^v, respectively. Moreover, $P^{pump,+}_{m,i}$, $P^{pump,-}_{m,i}$ and $P^{probe,+}_{m,i}$, $P^{pump,-}_{m,i}$ represent the optical CW forward (+) and backward (-) pump power and the probe power, respectively. $f^{c}_{g_{n.i}}$, $f^{c}_{e_{n.i}}$, $f^{v}_{g_{n.i}}$, and $f^{v}_{e_{n.i}}$ represent the corresponding carrier occupation probabilities respectively. Besides, the number of electrons associated with their corresponding occupation probabilities is calculated by $n^{c(v)}_{g_{n,i}}(z,t)=f^{e(v)}_{g_{n,i}}(z,t)N^{c(v)}_{G_i}$, $n^{c(v)}_{e_{n,i}}(z,t)=f^{c(v)}_{e_{n,i}}(z,t)N^{c(v)}_{E_i}$. In these equations, $N^{c(v)}_{G_i}$ and $N^{c(v)}_{E_i}$ represents the total number of electrons in each state, GS^c, ES^c, GS^v, and ES^v, respectively. For the *n*-th group of the GS and ES the maximum permitted carrier numbers are provided by

$$N^{c(v)}_{E_i}=N_{QD,i}D^{c(v)}_{e}V_d \quad (11)$$

$$N^{c(v)}_{G_i}=N_{QD,i}D^{c(v)}_{g}V_d \quad (12)$$

Here, $N_{QD,i}$,i is the density of QDs and V_d is the volume of the active region for both channels. The degeneracy of the GS and the ES states in the conduction

(valence) band are referred to as as $D_g^{c(v)}$, and $D_e^{c(v)}$, respectively[52–54]. The time constants corresponding to these carrier transition processes are called $\tau_{ge}{}^{v}$ (electron decay time from the GS^v to the ES^v), $\tau_{eg}{}^{c}$ (electron decay time from the ES^c to the GS^c), τ_{gr} (carrier lifetime from the GS^c to the GS^v), τ_{er} (carrier lifetime from the ES^c to the ES^v), the time constants according to FRET mechanism are illustrated as $\tau_{down\text{-}trans\text{-}g(e)}$ (electron transition time from the GS^c (ES^c) of channel-1 to the GS^c (ES^c) of channel-2) and $\tau_{up\text{-}trans\text{-}g(e)}$ (electron transition time from the GS^c (ES^c) of channel-2 to the GS^c (ES^c) of channel-1). Furthermore, the time constants related to the electron escape process in the valence and the conduction bands are acquired as

$$\tau_{ge}{}^{c(v)} = \tau_{eg}{}^{c(v)} \frac{D_g^{c(v)}}{D_e^{c(v)}} \exp(\Delta E_{eg}{}^{c(v)} / KT) \tag{13}$$

where $\Delta E_{eg}^{c(v)}$ is the energy interval between $ES^{c(v)}$ and $GS^{c(v)}$ [55, 57]. Degeneracies are determined by $D_g^c = 1$, $D_e^c = 3$, $D_g^v = 1$, and $D_e^v = 3$. As mention before, FRET process can result in carrier transfer in the conduction band which is modeled by the following transfer rate equation

$$W_{12,n,i}^{l} = \frac{2}{V_{eff}} \frac{e^2}{\hbar (n_i^p)^2 \varepsilon_0} E_{12,n}^{l} |< \Psi_{l,1}^{c} | \hat{e}.\hat{r} | \Psi_{l,2}^{c} >|^2 \\ B_{m,n}(E_{12,m}^{l} - E_{12,n}^{l}) G(E_{12,n}^{l}) \quad l = GS^c, ES^c \tag{14}$$

where $E_{12}^{l} = E_1^{l} - E_2^{l}$, and V_{eff} is the effective volume of QDs with different sizes. In the coupled rate equations, $\tau_{up(down)\_trans}^{l} = 1/W_{12,n}^{l}$ are the time constants for the transition between two QDs of various sizes. The linear material gain at *m*-th photon mode in Eqs. (1), (2), (5), (9) and (10), is provided by

$$g_{m,i}^{T}(t) = \int_0^L [\sum_{n=1}^{2M+1} g_{m,n,i}^{probe} (f_{g_{n,i}}^{c}(z,t) - f_{g_{n,i}}^{v}(z,t))] dz \tag{15}$$

where the linear optical gain resulting from stimulated recombination, transitioning from the *n*-th QD group of GS^c to the *m*-th photon mode of GS^v by applying probe power is determined by

$$g_{m,n,i}^{probe} = \frac{2}{V_{QD,i}} \frac{e^2}{cn_i^{probe} \hbar \varepsilon_0} E_{n,i}^{probe} |< \Psi_{g,i}^{c} | \hat{e}.\hat{r} | \Psi_{g,i}^{v} >|^2 \\ G_i(E_{n,i}^{probe}) B_{m,n}(E_{n,i}^{probe} - E_{m,i}^{probe}) \tag{16}$$

In this context, n_i^{probe} represents the refractive index related to probe

wavelengths, $V_{QD,i}$ is the volume of the QD and the term $|<\Psi^{c}_{g,i}|\hat{e}.\hat{r}|\Psi^{v}_{g,i}>|$ indicates the interband transition dipole moment. The ratio of the inhomogeneously expanded electron (hole) states is referred to as $G_i(E^{probe}_{n,i})$. The Gaussian distribution (G_i) can be accurately represented by the following equation to determine the IHB for the GS and ES

$$G_i(E^{p}_{n,i}) = \frac{1}{\sqrt{2\pi}\xi_0}\exp\left[\frac{-\left(E^{p}_{n,i}-E^{p}_{0,i}\right)^2}{2\xi_0^{\,2}}\right] \tag{17}$$

In which $E^{p}_{n,i} = E^{p}_{0,i} - (M+1-n)\Delta E \quad n=1,...,2M+1 \quad i=1,2 \quad p=\text{pump, probe}$. In the modeling framework, $E^{p}_{0,i}$ denotes the transfer energy of the most probable size within the QDs (*M+1*-th QD group). The index *i* is fixed at 1 for channel-1 and 2 for channel-2. Moreover, ξ_0 denotes the QD coverage and is defined as, $\xi_0=(1/2.35)^{\Gamma_{IHB}}$, where Γ_{IHB} =20 meV is the full width of half maximum (FWHM) of the Gaussian profile [38]. Observations based on simulation results reveal alterations in QD sizes from the two central radii (3 nm and 3.75 nm) by ΔR, corresponding to an energy difference of Γ_{IHB} which will result in IHB of the QD with different radii. Furthermore, intrinsic factors, such as pressure or temperature, induce interactions between carrier-carrier and phonon-carrier, homogeneously affecting all groups. This results in the manifestation of homogeneous broadening (HB) on the energy levels, modeled by a Lorentzian profile (Eq. (16)) with Γ_{HB} =20 meV as its FWHM at room temperature [52, 57].

$$B_{m,n}(E^{p}_{n,i}-E^{p}_{m,i}) = \frac{1}{\pi}\frac{\Gamma_{HB}/2}{\left(E^{p}_{n,i}-E^{p}_{m,i}\right)^2+(\Gamma_{HB}/2)^2} \tag{18}$$
$$n=1,...,2M+1, \quad m=\text{number of photon modes}$$

In Eqs. (3-4),(6-8), by considering the acquired broadenings, the linear interband absorption coefficient from ES^{v} to ES^{c}, resulting from the applied pump power, is as following [53]

$$\alpha^{T}_{m,i}(t) = \int_0^L [\sum_{n=1}^{2M+1} \alpha^{pump}_{m,n,i}(f^{v}_{e_{n,i}}(z,t) - f^{c}_{e_{n,i}}(z,t))]dz \tag{19}$$

Here the m-th photon mode's linear optical gain from the n-th QD group's ES is referred to as

$$\alpha_{m,n,i}^{Pump} = \frac{2}{V_{QD,i}} \frac{e^2}{c\varepsilon_0 n_i^{pump} \hbar} E_{n,i}^{pump} |< \Psi_{e,i}^{v} | \hat{e}.\hat{r} | \Psi_{e,i}^{c} >|^2 \\ G_i(E_{n,i}^{pump}) B_{m,n}(E_{n,i}^{pump} - E_{m,i}^{pump}) \quad (20)$$

In these equations, c represents the free space light speed, ε_0 is the free space permittivity, n_i^{pump} is the refractive index related to pump wavelengths, ħ is the reduced Planck's constant, *e* is the electron charge and $V_{QD,i}$ is the volume of the QD [58-62]. The term $|< \Psi_{e,i}^{v} | \hat{e}.\hat{r} | \Psi_{e,i}^{c} >|$ represents the interband transition dipole moment [42],[54-57] .

4. Result And Discussion

The presented results in Fig. 2 reveal the gain characteristics of QD-SOA and QD-RSOA under varying pump powers and waveguide lengths, highlighting key differences in their performance. By varying the pump power of channel 1 in SOA and RSOA, the gain of channel 1 initially increased and then saturated to a final value. The graphs show changes in channel-1 gain with blue lines and channel-2 gain with orange ones. In Fig. 2(a), it is evident that both channels experience an increase in gain in response to pump power, starting at a low value. This trend continues until pump-1 reaches 100 mW and pump-2 ,150 mW, after which the gain levels is saturated. This stabilization is due to the saturation of carriers in the conduction band, resulting in a constant optical gain. The minimum required pump power for channel-1 is about 100 mW. Varying the pump power of channel-2 is not expected to affect the gain of channel-1 significantly, but there may be slight changes due to carrier transfer between QDs of different sizes. And this slight change will lead to a rise as the channel-2 pump power increases. By changing the pump power of channel-1, the gain of channel-2 will also change slightly. This will be due to carrier transfer between QDs with different radii. In Fig. 2(a) and 2(b), where the pump power is varied on channel-1 while keeping channel-2 constant, QD-RSOA exhibits a higher gain than QD-SOA, demonstrating its superior amplification efficiency at higher pump powers. Additionally, increasing the waveguide length from L=1000 μm (Fig. 2a) to L=2000 μm (Fig. 2b) leads to higher gains for both channels. This can be attributed to the extended interaction region in longer waveguides, allowing for enhanced carrier-photon interaction. In addition, the minimum power necessary to have the required gain increases to 150 mW.

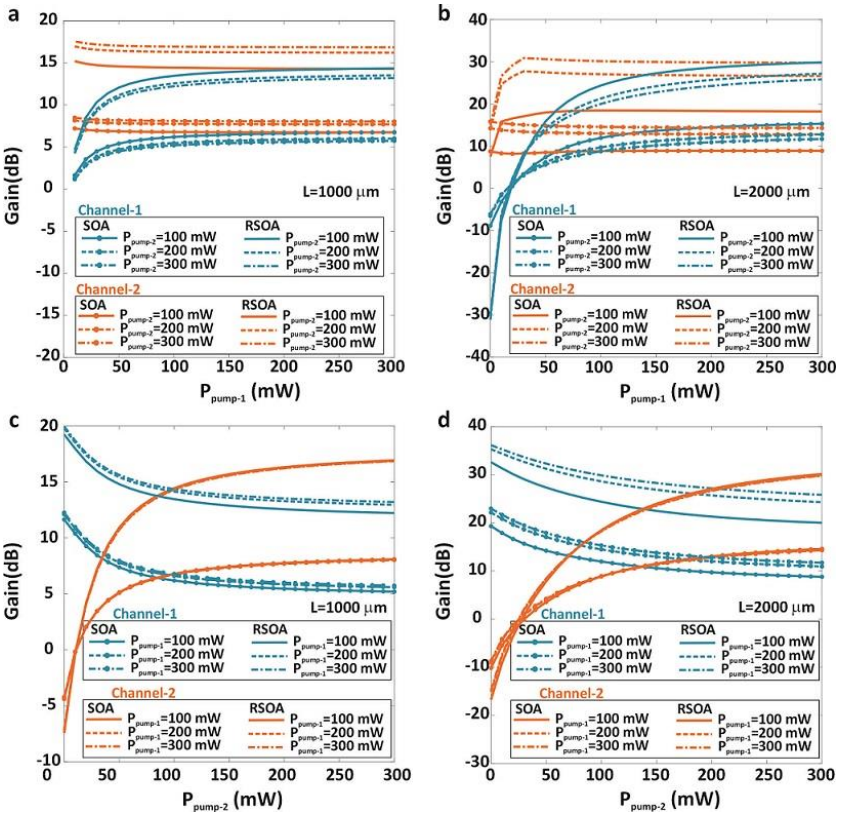

Fig. 2. The optical gain dependence on input pump power is investigated for both QD-SOA and QD-RSOA devices. The analysis considers the optical gain in channel-1 and channel-2 under different conditions. First, the gain is examined while varying the pump power applied to channel-1, keeping the pump power for channel-2 constant, for two device lengths: **a)** L=1000μm and **b)** L=2000μm. Similarly, the optical gain is assessed when the pump power applied to channel-2 is varied, while maintaining a constant pump power for channel-1, at **c)** L=1000μm and **d)** L=2000μm. (In all cases, the input probe power applied to both channels is set to −20dBm).

This simulation further reveals how the channel gains fluctuate under constant power conditions, primarily due to the influence of the Förster Resonance Energy Transfer (FRET) process. These fluctuations are particularly evident when the power input to channel-2 is low, and population inversion within the structure has not yet been achieved. In this state, carriers predominantly occupy the valence band (VB) rather than transitioning to the conduction band (CB).

Under such conditions, the optical signal from the probe promotes the

absorption of carriers from the VB to the CB. This activity increases the carrier population in channel-2, facilitated by the FRET process, which enables energy or carrier exchange between quantum dots (QDs) of different sizes. As the input power to channel-2 rises and the carrier distribution between the CB and VB shifts, stimulated emission is triggered. However, as the power input reaches higher levels, the absorption diminishes, and both channels stabilize, achieving their respective gain values.

The optical gain fluctuations in channel-1 are notably more pronounced than those in channel-2. This disparity arises because the FRET process tends to preferentially transfer carriers from QDs with smaller radii to those with larger radii, amplifying the dynamic interactions within channel-1. These findings underscore the intricate interplay of carrier dynamics, FRET effects, and power input levels in determining the performance and stability of quantum dot-based optical amplifiers.

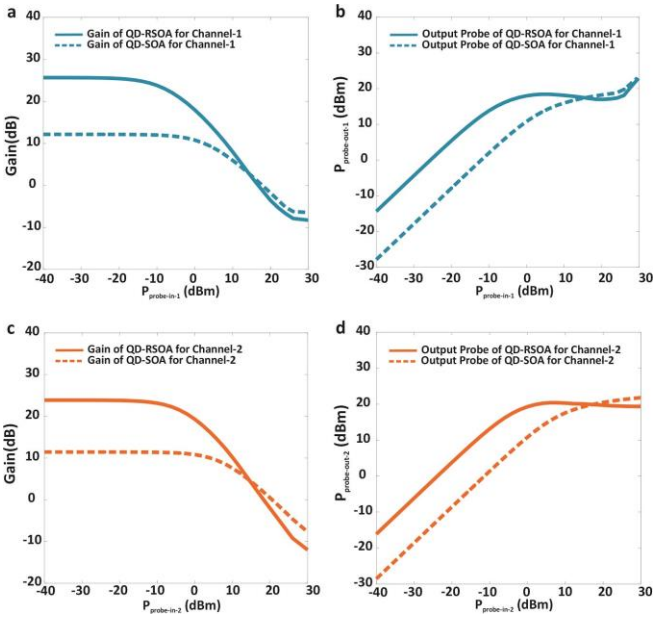

Fig. 3. The optical gain and output probe power are analyzed as functions of input probe power for both QD-SOA and QD-RSOA devices. **a)** The optical gain and **b)** the output probe power for channel-1 are evaluated with varying input probe power applied to channel-1 while maintaining constant pump power for channel-1. **c)** The optical gain and **d)** The output probe power for channel-2 are examined with varying input probe power applied to channel-2, while keeping the pump power for channel-1 constant.

Similarly, in Fig. 2(c) and 2(d), where the pump power is varied on channel-2 while keeping channel-1 constant, the gain trends are consistent with those in Fig. 2(a) and 2(b). QD-RSOA consistently achieves higher gain than QD-SOA across both waveguide lengths. The longer waveguide (L=2000 μm, Fig. 2(d)) results in greater gain compared to the shorter waveguide (L=1000 μm, Fig. 2(c)). Across all scenarios, the results also show that the gain saturation point shifts with the applied pump power, and the overall gain is influenced by the pump power applied to both channels. These findings emphasize that QD-RSOA is better suited for applications requiring higher gain and longer waveguides enhance the amplification efficiency for both QD-SOA and QD-RSOA. Based on evaluations outlined in Fig. 2, pump 1 and pump 2 were set at 150 mW for a cavity length of 2000 μm. The probe power for both channels was -20 dBm, with inhomogeneous and homogeneous broadening equal to 20 meV.

The analysis of the gain and output probe power characteristics versus input probe power under constant pump powers for dual-wavelength all-optical QD-SOA and QD-RSOA, as illustrated in Fig. 3, highlights important performance distinctions. In Fig. 3(a) and 3(c), the optical gain for channel-1 and channel-2, respectively, shows a noticeable trend: both QD-SOA and QD-RSOA experience gain compression as the input probe power increases. However, QD-RSOA consistently achieves a higher gain compared to QD-SOA across the range of input powers. This underscores QD-RSOA's superior amplification capability at moderate to high input probe powers. For QD-SOA and QD-RSOA, the maximum input probe power before gain reduction is 5 dBm and -10 dBm, respectively on channel-1. For channel 2, with the maximum input probe power being 10 dBm for QD-SOA and 0 dBm for QD-RSOA. The reduction in gain with increasing input power reflects the saturation effects inherent in both devices, driven by carrier depletion.

Fig. 3(b) and 3(d) reveal the output probe power characteristics for channel-1 and channel-2, respectively. Both QD-SOA and QD-RSOA exhibit a linear increase in output power at low input probe powers, transitioning to saturation at higher input levels. The output probe power for QD-RSOA surpasses that of QD-SOA, reaffirming its stronger amplification performance. These results demonstrate that QD-RSOA maintains higher output efficiency compared to QD-SOA under similar operating conditions.

The Modulation-Cancellation Dynamic Range (MCDR) is a crucial parameter defined as the range of input power within which the variation in output power remains below 1 dB [4]. A large MCDR is highly desirable, especially for applications such as power equalization and modulation cancellation, which are

essential in wavelength reuse systems [13, 14]. A higher MCDR allows for a more stable operation across a broader power range, making it beneficial for various optical communication systems.

When comparing QD-RSOAs to QD-SOAs, the former typically exhibits smaller output power variations, which directly contributes to a greater MCDR. As illustrated in Fig. 3(b) and 3(d), the output probe power as a function of the input probe power shows that the MCDR for QD-RSOAs exceeds that of QD-SOAs. While QD-SOAs may demonstrate higher saturation output power, this advantage is counterbalanced by the fact that the MCDR for QD-RSOAs is observed across a wider range of input powers.

In contrast, the MCDR for QD-SOAs tends to only be significant at relatively higher input power levels. Therefore, while QD-SOAs can provide higher saturation output power, QD-RSOAs offer a more consistent performance across a broader power range, making them more suitable for applications requiring precise modulation cancellation and power stabilization, as noted in [13, 14].

These results demonstrate the performance trade-offs between QD-SOA and QD-RSOA, with QD-RSOA offering better gain and output power capabilities, making it more suitable for applications requiring high amplification. Conversely, QD-SOA, with its lower gain and saturation power, may find applications in scenarios where moderate gain and reduced power consumption are desirable.

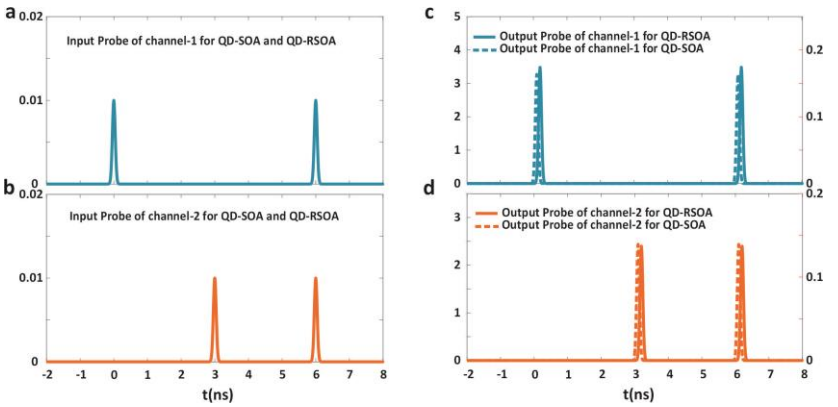

Fig. 4. The performance of the proposed dual-wavelength all-optical QD-SOA and QD-RSOA is analyzed. This includes the temporal evolution of the input probe power for **a)** channel-1 and **b)** channel-2. Additionally, the temporal evolution of the output probe power is examined for **c)** channel-1 and **d)** channel-2 where the right vertical axis corresponds to SOA, while the left vertical axis is attributed to RSOA.

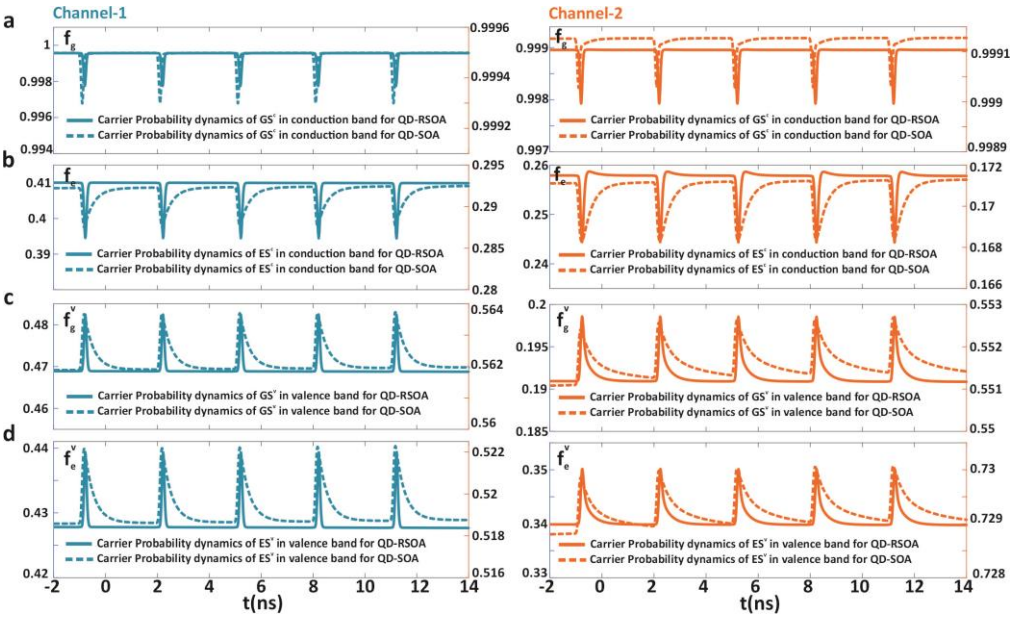

Fig. 5. The carrier probability dynamics of the dual-wavelength all-optical QD-SOA and QD-RSOA are evaluated over time. This includes the temporal analysis of carrier probability for **a)** GS and **b)** ES in CB for channel-1 and channel-2. The temporal evaluation of carrier probability of **c)** GS and **d)** ES in VB for channel-1 and channe-2. In all figures, the right vertical axis corresponds to SOA, while the left vertical axis is attributed to RSOA.

The temporal evolution of input and output probe power for the dual-wavelength all-optical QD-SOA and QD-RSOA systems is presented in Fig. 4, highlighting their performance in handling dual-channel signals. Fig. 4(a) and 4(b) depict the input probe power profiles for channel-1 and channel-2, respectively. Both input signals exhibit well-defined, periodic pulse shapes, indicating consistent and controlled signal injection for testing the devices under dual-channel operation. At time t1, the input optical pulse is directed solely to channel-1, resulting in the amplified output being found only in channel-1 output. Subsequently, at time t2, the input probe's optical pulse is exclusively sent to channel-2, leading to the observation of the amplified output only for channel-2. Ultimately, at time t3, an optical pulse is simultaneously applied as an input probe to both channels, with the amplified signal for both channels being available at the output. Fig. 4(c) and 4(d) illustrate the output probe power for channel-1 and channel-2, respectively, where the right vertical axis corresponds to SOA, while the left vertical axis is attributed to RSOA. For both

channels, the QD-SOA and QD-RSOA successfully amplify the input signals, maintaining the temporal characteristics of the pulses. However, notable differences are observed in the amplification levels. The QD-RSOA demonstrates superior amplification performance, evident in its higher peak output power compared to the QD-SOA for both channels. In contrast, QD-SOA outputs exhibit slightly lower peak power, reflecting its moderate amplification performance. The results confirm the suitability of both QD-SOA and QD-RSOA for dual-wavelength applications, with QD-RSOA showing higher efficiency in signal amplification. These findings underscore the potential of QD-RSOA for high-performance, multi-channel optical communication systems, whereas QD-SOA may cater to applications prioritizing reduced complexity and power consumption. Input probe power is set at -10 dBm with a pump power of 150 mW and an average value of 20 meV for both channels. This aligns with the earlier results that emphasize the higher gain and output power capabilities of QD-SOA.

The temporal evolution of carrier probability dynamics for dual-wavelength all-optical QD-SOA and QD-RSOA systems provides critical insights into their operational characteristics for both CB and VB transitions. The carrier dynamics are analyzed for the GS and ES in channel-1 and channel-2, as depicted in the Fig. 5. In this Fig., the right vertical axis corresponds to SOA, while the left vertical axis is attributed to RSOA. For channel-1, the carrier probabilities in the CB for GS and ES (Fig. 5(a) and 5(b)) exhibit periodic modulation in response to the injected signal. The QD-SOA shows slightly lower carrier depletion compared to QD-RSOA, indicating a less efficient carrier extraction process. This difference reflects the distinct gain mechanisms and carrier recombination dynamics between the two devices. Similar behavior is observed in the VB for GS and ES (Fig. 5(c) and 5(d)), with QD-RSOA demonstrating more pronounced carrier depletion and recovery, aligning with its higher amplification performance. For channel-2, the carrier probability dynamics (Fig. 5(e), 5(f), 5(g), and 5(h)) follow a similar trend as channel-1, with periodic carrier modulation corresponding to the input signal pulses. Again, QD-RSOA outperforms QD-SOA in terms of carrier depletion, particularly in the GS of both CB and VB. This highlights the QD-RSOA's ability to handle dual-wavelength signals more effectively, ensuring stronger signal amplification and more efficient carrier utilization. The results collectively emphasize the superior carrier dynamics of QD-RSOA over QD-SOA for dual-wavelength operations. The QD-RSOA exhibits better carrier extraction and recovery, enabling higher gain and more consistent amplification across both channels. These findings

demonstrate the potential of QD-RSOA for high-performance multi-channel optical systems, while QD-SOA may find applications where moderate performance suffices and simplicity or cost-effectiveness is prioritized.

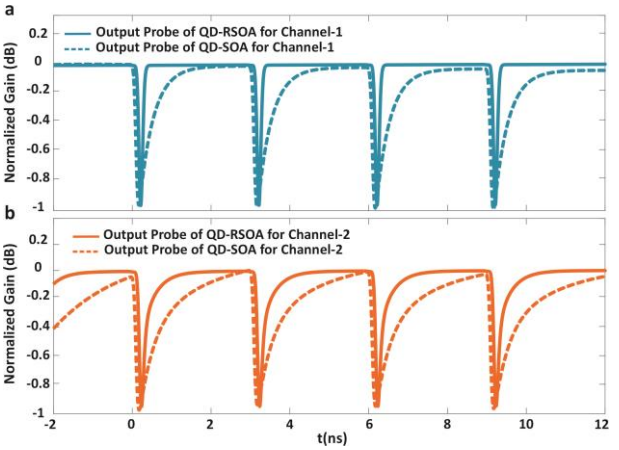

Fig. 6. The temporal evaluation of the normalized optical gain for the dual-wavelength all-optical QD-SOA and QD-RSOA is presented for **a)** channel-1 and **b)** channel-2.

The normalized optical gain dynamics for both QD-RSOA and QD-SOA presented in Fig. 6 exhibit distinct features, particularly in terms of modulation depth and recovery time. For Channel-1 (Fig. 6(a)), the QD-RSOA demonstrates steeper gain recovery after depletion, indicating a more efficient carrier replenishment process. This faster recovery suggests that QD-RSOAs are better suited for high-speed optical communication systems where rapid gain modulation is required. In contrast, the QD-SOA shows slower recovery, which may lead to signal degradation in high-speed operations. For Channel-2 (Fig. 6(b)), the gain dynamics remain consistent with those observed for Channel-1, with QD-RSOA exhibiting a more pronounced modulation depth. This behavior can be attributed to the enhanced feedback mechanism within the reflective configuration of QD-RSOAs, which optimizes carrier depletion and replenishment cycles. The higher gain modulation depth for QD-RSOAs also points to their ability to provide greater signal integrity and amplification in dual-wavelength systems.

The rapid gain recovery time observed in QD-RSOAs can be attributed to two primary factors. The first factor occurs when a single pulse is introduced into the structure, causing carriers in the ground state to recombine through stimulated emission. This recombination process leads to the excitation of carriers in the

excited state, which then replenishes the ground state, essentially acting as a reservoir for carriers. This cycle facilitates a rapid recovery of gain, enabling quicker device response times.

Secondly, optical pumping plays a critical role in maintaining this fast recovery. During optical pumping, carriers are injected into the excited state through absorption, a process that can be controlled by adjusting the optical pumping intensity. This provides a continuous supply of carriers to support the gain recovery. Additionally, the carriers' relaxation from the wetting layer contributes to the refilling of the excited state, further enhancing the recovery dynamics. As the optical pumping power increases, more carriers are absorbed, and the system reaches a steady state more quickly. This results in a reduced recovery time, as the higher pump power accelerates the replenishment of carriers, ensuring faster stabilization of the system. These mechanisms collectively drive the rapid gain recovery times in QD-RSOAs, making them highly suitable for high-speed optical applications. Furthermore, at higher input powers, there is an increase in the number of carriers recombining radiatively. Additionally, it should be noted that RSOAs have two recovery regions instead of one as seen in traditional traveling SOAs. This is due to both the input and output facets being located at the same point (z = 0) in RSOAs. The first recovery area is where the input signal is first introduced, while the second area is where the backward signal exits the device.

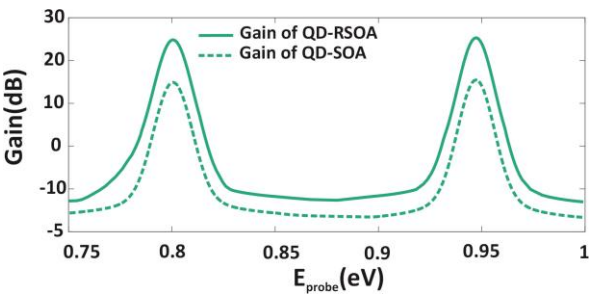

Fig. 7. The optical gain spectrum for QD-SOA and QD-RSOA

The optical gain as a function of probe energy (wavelength) reveals two distinct gain peaks corresponding to resonant energy transitions in the QD structure. It can be seen that there are two distinct wavelengths in which gain has non-zero value. One is 0.8 eV at 1.55 μm and the other is 0.95 eV at the wavelength of 1.31 μm, and no gain at the other wavelengths or energies are present. The QD-RSOA consistently outperforms the QD-SOA across the

observed energy range, with higher peak gains and a broader gain spectrum. This superior performance highlights the enhanced amplification capabilities of QD-RSOAs, which are essential for WDM applications. The sharper and higher gain peaks observed in QD-RSOAs can be attributed to the reflective architecture, which enables more efficient interaction between the optical signals and the quantum dot active region. In contrast, the QD-SOA exhibits lower peak gain and a narrower gain spectrum, limiting its application in scenarios requiring broader bandwidth or higher signal amplification.

The comparative analysis of all-optical QD-SOA and QD-RSOA presented in this study highlights the distinct advantages and limitations of each device in dual-wavelength optical systems. Across both channels, QD-RSOA consistently demonstrates faster gain recovery following depletion and greater modulation depth. This behavior can be attributed to the reflective configuration of the QD-RSOA, which facilitates more efficient carrier replenishment by confining the optical signals within the active region. Such fast recovery dynamics make QD-RSOAs particularly well-suited for high-speed optical communication systems where rapid gain modulation is required. In contrast, the QD-SOA exhibits a slower recovery rate and reduced modulation depth, reflecting less efficient carrier dynamics. While still viable for optical amplification, these characteristics may limit QD-SOAs in applications requiring rapid signal modulation or systems with stringent speed requirements. The comparatively gradual recovery observed in QD-SOAs could also lead to higher susceptibility to signal distortion and cross-talk in densely populated WDM systems. The spectral gain profiles for both devices highlight key differences in their amplification capabilities across a range of probe energies. QD-RSOAs consistently outperform QD-SOAs in terms of peak gain, with sharper and more pronounced gain peaks. Furthermore, the QD-RSOA demonstrates a broader gain bandwidth, making it advantageous for WDM applications requiring amplification over a wide spectral range. The reflective architecture of the QD-RSOA plays a significant role in its superior spectral performance. By enabling better interaction between the optical signals and the QD active region, this configuration allows for more efficient utilization of carriers, resulting in higher peak gains and broader amplification. In comparison, QD-SOAs exhibit lower peak gains and narrower spectral responses, which could limit their deployment in broadband or high-performance optical systems. The comparative performance of QD-SOAs and QD-RSOAs underscores the importance of device selection based on application-specific requirements. QD-RSOAs emerge as the preferred choice for high-speed and multi-channel optical systems, where fast gain recovery, high modulation depth, and broad spectral response are critical. Their reflective configuration also enhances signal

integrity and reduces cross-talk, addressing key challenges in dual-wavelength and WDM systems. On the other hand, QD-SOAs, with their relatively simpler architecture, may still find use in cost-sensitive applications or systems with less demanding speed and bandwidth requirements. Their performance, while limited compared to QD-RSOAs, remains adequate for certain optical amplification tasks where absolute speed and spectral breadth are not primary concerns. The results of this study pave the way for further research into the optimization and application of QD-RSOAs in advanced optical networks. Future work could focus on scaling QD-RSOAs for multi-channel WDM systems, investigating their performance under varying input power and wavelength conditions, and exploring their integration with other photonic components for compact and efficient optical modules. Meanwhile, improvements in QD-SOA design and carrier dynamics could enhance their utility in niche applications requiring lower-cost solutions.

In conclusion, the QD-RSOA outperforms the QD-SOA in nearly all performance metrics critical to modern optical communication systems, making it a superior choice for demanding applications. However, the QD-SOA retains its value in specific contexts, ensuring its relevance in the broader landscape of optical amplification technologies.

5. CONCLUSIONS

This study presented the design and performance analysis of a dual-wavelength all-optical QD-RSOA, operating at 1.31 μm and 1.55 μm wavelengths. By leveraging solution-processed InAs/AlAs QDs and employing optical pumping, the QD-RSOA achieves significant advancements over conventional optically pumped QD-SOAs. The reflective architecture enhances carrier replenishment, enabling faster gain recovery, broader gain bandwidth, and higher modulation depth, which are critical for modern optical communication systems. Numerical simulations validated the superior performance of the QD-RSOA in terms of gain efficiency, spectral response, and operational robustness. The dual-wavelength capability facilitates simultaneous or independent signal amplification, making the device particularly suited for WDM and all-optical signal processing applications. The findings underscore the QD-RSOA's potential as a high-performance solution for multi-channel and high-speed optical networks. Future research could focus on optimizing the device for large-scale deployment and exploring its integration with other photonic components to create compact, cost-effective modules for advanced optical communication systems.

6. REFERENCES

[1] M. Heydari, A. R. Zali, R. E. Gildeh and A. Farmani, "Fully Integrated, 80 GHz Bandwidth, 1.3μ m InAs/InGaAs CW-PW Quantum Dot Passively Colliding-Pulse Mode-Locked (CPM) Lasers for IR Sensing Application," in *IEEE Sensors Journal*, vol. 22, no. 7, pp. 6528-6535, 1 April1, 2022, doi: 10.1109/JSEN.2022.3153656.

[2] M. Heydari, A. R. Zali, R. E. Gildeh and A. Farmani, "Fully Integrated, 80 GHz Bandwidth, 1.3μ m InAs/InGaAs CW-PW Quantum Dot Passively Colliding-Pulse Mode-Locked (CPM) Lasers for IR Sensing Application," in IEEE Sensors Journal, vol. 22, no. 7, pp. 6528-6535, 1 April1, 2022, doi: 10.1109/JSEN.2022.3153656.

[3] Ali Farmani, Mahmoud Farhang, Mohammad H. Sheikhi, "High performance polarization-independent Quantum Dot Semiconductor Optical Amplifier with 22dB fiber to fiber gain using Mode Propagation Tuning without additional polarization controller," Optics & Laser Technology,Volume 93,2017,Pages 127-132,ISSN 0030-3992, https://doi.org/10.1016/j.optlastec.2017.02.007.

[4] M. Sugawara, T. Akiyama, N. Hatori, Y. Nakata, H. Ebe, and H. Ishikawa, "Quantum-dot semiconductor optical amplifiers for high-bit-rate signal processing up to 160 Gb s-1and a new scheme of 3R regenerators," Measurement Science and Technology, vol. 13, no. 11, pp. 1683–1691, Oct. 2002, doi: 10.1088/0957-0233/13/11/304.

[5] Y. B. Ezra, B. I. Lembrikov, and M. Haridim, "Ultrafast All-Optical processor based on Quantum-Dot semiconductor optical amplifiers," IEEE Journal of Quantum Electronics, vol. 45, no. 1, pp. 34–41, Nov. 2008, doi: 10.1109/jqe.2008.2003497.

[6] F. S. Nahaei, A. Rostami, and S. Matloub, "Selective band amplification in ultra-broadband superimposed quantum dot reflective semiconductor optical amplifiers," Applied Optics, vol. 61, no. 15, p. 4509, May 2022, doi: 10.1364/ao.427496.

[7] J. Gomis et al., "Ultrafast Gain Recovery in Quantum Dot based Semiconductor Optical Amplifiers," Optica Publishing Group, p. 1, Jun. 2007, doi: 10.1109/cleoe-iqec.2007.4386291.

[8] E. A. Viktorov et al., "Recovery time scales in quantum dot devices," Eur. Conf. Lasers Electro-Optics, Optica Publishing Group, p. 1, Jun. 2009, doi: 10.1109/cleoe-eqec.2009.5191460.

[9] C. Meuer et al., "Static gain saturation in quantum dot semiconductor optical amplifiers," Optics Express, vol. 16, no. 11, p. 8269, May 2008, doi: 10.1364/oe.16.008269.

[10] V. Uskov, T. W. Berg, and J. Mork, “Theory of Pulse-Train amplification without patterning effects in Quantum-Dot semiconductor optical Amplifiers,” IEEE Journal of Quantum Electronics, vol. 40, no. 3, pp. 306–320, Mar. 2004, doi: 10.1109/jqe.2003.823032.

[11] S. M. Izadyar, M. Razaghi, and A. Hassanzadeh, “Quantum dot semiconductor optical amplifier: role of second excited state on ultrahigh bit-rate signal processing,” Applied Optics, vol. 56, no. 12, p. 3599, Apr. 2017, doi: 10.1364/ao.56.003599.

[12] H. A. Yazbeck, V. V. Belyaev, I. M. Tkachenko, and M. M. Hamze, “Multi-electrode quantum-dot semiconductor optical amplifier as an intensity modulator of signals in optical communication systems,” Journal of Physics Conference Series, vol. 1560, no. 1, p. 012021, Jun. 2020, doi: 10.1088/1742-6596/1560/1/012021.

[13] J.-L. Xiao and Y.-Z. Huang, “Numerical analysis of gain saturation, noise Fig., and carrier distribution for Quantum-Dot Semiconductor-Optical amplifiers,” IEEE Journal of Quantum Electronics, vol. 44, no. 5, pp. 448–455, Mar. 2008, doi: 10.1109/jqe.2007.916683.

[14] T. W. Berg and J. Mork, “Saturation and noise properties of quantum-dot optical amplifiers,” IEEE Journal of Quantum Electronics, vol. 40, no. 11, pp. 1527–1539, Oct. 2004, doi: 10.1109/jqe.2004.835114.

[15] L. Huang, W. Hong, and G. Jiang, “All-optical power equalization based on a two-section reflective semiconductor optical amplifier,” Optics Express, vol. 21, no. 4, p. 4598, Feb. 2013, doi: 10.1364/oe.21.004598.

[16] S. Ó. Dúill et al., “Efficient modulation cancellation usingreflective SOAs,” Optics Express, vol. 20, no. 26, p. B587, Dec. 2012, doi: 10.1364/oe.20.00b587.

[17] W. Zhan, P. Zhou, Y. Zeng, M. Mukaikubo, T. Tanemura, and Y. Nakano, “Optimization of Modulation-Canceling reflective Semiconductor Optical Amplifier for colorless WDM transmitter applications,” Jan. 15, 2017. https://opg.optica.org/jlt/abstract.cfm?uri=jlt-35-2-274

[18] J. P. Babic, A. R. Totovic, J. V. Crnjanski, M. M. Krstic, M. L. Masanovic, and D. M. Gvozdic, “Enhancement of the MQW-RSOA’s Small-Signal modulation bandwidth by inductive peaking,” Journal of Lightwave Technology, vol. 37, no. 9, pp. 1981–1989, Feb. 2019, doi: 10.1109/jlt.2019.2896914.

[19] P. G. Eliseev and V. Van Luc, “Semiconductor optical amplifiers: multifunctional possibilities, photoresponse and phase shift properties,” Pure and Applied Optics Journal of the European Optical Society Part A, vol. 4, no. 4, pp. 295–313, Jul. 1995, doi: 10.1088/0963-9659/4/4/004.

[20] M. J. Connelly, “Wideband model of a reflective tensile-strained bulk semiconductor optical amplifier,” Proceedings of SPIE, the International Society for Optical Engineering/Proceedings of SPIE, vol. 9134, p. 91341R, May 2014, doi: 10.1117/12.2051657.
[21] C. Antonelli and A. Mecozzi, “Reduced model for the nonlinear response of reflective semiconductor optical amplifiers,” IEEE Photonics Technology Letters, vol. 25, no. 23, pp. 2243–2246, Sep. 2013, doi: 10.1109/lpt.2013.2282215.
[22] Z. Vujicic, R. P. Dionisio, A. Shahpari, N. B. Pavlovic, and A. Teixeira, “Efficient dynamic modeling of the reflective semiconductor optical amplifier,” IEEE Journal of Selected Topics in Quantum Electronics, vol. 19, no. 5, pp. 1–10, Apr. 2013, doi: 10.1109/jstqe.2013.2259616.
[23] E. Zhou, X. Zhang, and D. Huang, “Analysis on dynamic characteristics of semiconductor optical amplifiers with certain facet reflection based on detailed wideband model,” Optics Express, vol. 15, no. 14, p. 9096, Jan. 2007, doi: 10.1364/oe.15.009096.

[24] C. Antonelli, A. Mecozzi, Z. Hu, and M. Santagiustina, “Analytic study of the modulation response of reflective semiconductor optical amplifiers,” Journal of Lightwave Technology, vol. 33, no. 20, pp. 4367–4376, Jul. 2015, doi: 10.1109/jlt.2015.2453232.
[25] R. Totovic, J. V. Crnjanski, M. M. Krstic, and D. M. Gvozdic, “Modeling of semiconductor optical amplifiers for optical access networks,” 2022 30th Telecommunications Forum (TELFOR), pp. 420–425, Nov. 2018, doi: 10.1109/telfor.2018.8612029.
[26] M. Mohamadzadeh, S. Matloub, and M. Faraji, “Simulation and design of dual-wavelength all-optical semiconductor optical amplifier with solution-processed quantum dots,” Optical Materials, vol. 150, p. 115230, Mar. 2024, doi: 10.1016/j.optmat.2024.115230.
[27] H. A. Yazbeck, V. V. Belyaev, I. M. Tkachenko, and M. M. Hamze, “Multi-electrode quantum-dot semiconductor optical amplifier as an intensity modulator of signals in optical communication systems,” Journal of Physics Conference Series, vol. 1560, no. 1, p. 012021, Jun. 2020, doi: 10.1088/1742-6596/1560/1/012021.
[28] J. L. Wei et al., “Wavelength reused bidirectional transmission of adaptively modulated optical OFDM signals in WDM-PONs incorporating SOA and RSOA intensity modulators,” Optics Express, vol. 18, no. 10, p. 9791, Apr. 2010, doi: 10.1364/oe.18.009791.

[29] Raja, K. Mukherjee, and J. N. Roy, "Analysis of new all optical polarization-encoded Dual SOA-based ternary NOT & XOR gate with simulation," Photonic Network Communications, vol. 41, no. 3, pp. 242–251, May 2021, doi: 10.1007/s11107-021-00932-0.
[30] Y. Zhao, Z. Yan, P. Fu, Y. Cai, and Y. Yuan, "All-optical wavelength conversion based on dual-polarization SOAs for a 112Gbps PDM-16QAM signal using parallel dual-pump," OSA Continuum, vol. 4, no. 4, p. 1125, Mar. 2021, doi: 10.1364/osac.415288.
[31] J. Gong et al., "All-optical wavelength conversion for mode division multiplexed superchannels," Optics Express, vol. 24, no. 8, p. 8926, Apr. 2016, doi: 10.1364/oe.24.008926.
[32] N. Calabretta, W. Miao, K. Mekonnen, and K. Prifti, "SOA based photonic integrated WDM Cross-Connects for optical Metro-Access networks," Applied Sciences, vol. 7, no. 9, p. 865, Aug. 2017, doi: 10.3390/app7090865.
[33] M. Virte and P. Marin-Palomo, "Integrated multi-wavelength lasers for all-optical processing of ultra-high frequency signals," Applied Physics Letters, vol. 123, no. 18, Oct. 2023, doi: 10.1063/5.0170499.
[34] F. D. Mahad, A. S. M. Supa'at, S. M. Idrus, and D. Forsyth, "Comparative performance testing of SOA wavelength conversion techniques for future all-optical systems," Optik, vol. 124, no. 12, pp. 1254–1259, May 2012, doi: 10.1016/j.ijleo.2012.03.002.
[35] F. Zarinetchi, S. P. Smith, and S. Ezekiel, "Stimulated Brillouin fiber-optic laser gyroscope," Optics Letters, vol. 16, no. 4, p. 229, Feb. 1991, doi: 10.1364/ol.16.000229.
[36] M. Ajiya, M. A. Mahdi, M. H. Al-Mansoori, S. Hitam, and M. Mokhtar, "Seamless tuning range based-on available gain bandwidth in multiwavelength Brillouin fiber laser," Optics Express, vol. 17, no. 8, p. 5944, Mar. 2009, doi: 10.1364/oe.17.005944.
[37] V. Uskov, J. McInerney, F. Adler, H. Schweizer, and M. H. Pilkuhn, "Auger carrier capture kinetics in self-assembled quantum dot structures," Applied Physics Letters, vol. 72, no. 1, pp. 58–60, Jan. 1998, doi: 10.1063/1.120643.
[38] P. Bhattacharya, D. Klotzkin, O. Qasaimeh, W. Zhou, S. Krishna, and D. Zhu, "High-speed modulation and switching characteristics of In(Ga)As-Al(Ga)As self-organized quantum-dot lasers," IEEE Journal of Selected Topics in Quantum Electronics, vol. 6, no. 3, pp. 426–438, May 2000, doi: 10.1109/2944.865098.
[39] H. Dortaj and S. Matloub, "Design and simulation of two-color mid-infrared photoconductors based on intersubband transitions in quantum

structures," Physica E Low-dimensional Systems and Nanostructures, vol. 148, p. 115660, Jan. 2023, doi: 10.1016/j.physe.2023.115660.
[40] H. Dortaj et al., "High-speed and high-precision PbSe/PbI2 solution process mid-infrared camera," Scientific Reports, vol. 11, no. 1, Jan. 2021, doi: 10.1038/s41598-020-80847-4.
[41] R. Debnath, O. Bakr, and E. H. Sargent, "Solution-processed colloidal quantum dot photovoltaics: A perspective," Energy & Environmental Science, vol. 4, no. 12, p. 4870, Jan. 2011, doi: 10.1039/c1ee02279b.
[42] F. P. G. De Arquer, A. Armin, P. Meredith, and E. H. Sargent, "Solution-processed semiconductors for next-generation photodetectors," Nature Reviews Materials, vol. 2, no. 3, Jan. 2017, doi: 10.1038/natrevmats.2016.100.
[43] Samuel, "Electrifying quantum dots for lasers," Nature Materials, vol. 17, no. 1, pp. 9–10, Nov. 2017, doi: 10.1038/nmat5040.
[44] P. Yu et al., "Absorption Cross-Section and related optical properties of colloidal INAS quantum dots," The Journal of Physical Chemistry B, vol. 109, no. 15, pp. 7084–7087, Mar. 2005, doi: 10.1021/jp046127i.
[45] M. Yuan, M. Liu, and E. H. Sargent, "Colloidal quantum dot solids for solution-processed solar cells," Nature Energy, vol. 1, no. 3, Feb. 2016, doi: 10.1038/nenergy.2016.16.
[46] O. Voznyy, B. R. Sutherland, A. H. Ip, D. Zhitomirsky, and E. H. Sargent, "Engineering charge transport by heterostructuring solution-processed semiconductors," Nature Reviews Materials, vol. 2, no. 6, May 2017, doi: 10.1038/natrevmats.2017.26.
[47] S. Hoogland, V. Sukhovatkin, I. Howard, S. Cauchi, L. Levina, and E. H. Sargent, "A solution-processed 1.53 μm quantum dot laser with temperature-invariant emission wavelength," Optics Express, vol. 14, no. 8, p. 3273, Jan. 2006, doi: 10.1364/oe.14.003273.
[48] H. Uesugi, M. Kita, and T. Omata, "Synthesis of size-controlled colloidal InAs quantum dots using triphenylarsine as a stable arsenic source," Journal of Crystal Growth, vol. 416, pp. 134–141, Feb. 2015, doi: 10.1016/j.jcrysgro.2015.01.031.
[49] M. Liu et al., "Lattice anchoring stabilizes solution-processed semiconductors," Nature, vol. 570, no. 7759, pp. 96–101, May 2019, doi: 10.1038/s41586-019-1239-7.
[50] R. Lakowicz, Principles of fluorescence spectroscopy. 2006. doi: 10.1007/978-0-387-46312-4.
[51] Chou and A. Dennis, "Förster Resonance Energy Transfer between Quantum Dot Donors and Quantum Dot Acceptors," Sensors, vol. 15, no. 6, pp. 13288–13325, Jun. 2015, doi: 10.3390/s150613288.

[52] F. Demangeot, D. Simeonov, A. Dussaigne, R. Butté, and N. Grandjean, “Homogeneous and inhomogeneous linewidth broadening of single polar GaN/AlN quantum dots,” Physica Status Solidi. C, Conferences and Critical Reviews/Physica Status Solidi. C, Current Topics in Solid State Physics, vol. 6, no. S2, Mar. 2009, doi: 10.1002/pssc.200880971.
[53] J. Jasieniak, L. Smith, J. Van Embden, P. Mulvaney, and M. Califano, “Re-examination of the Size-Dependent absorption properties of CDSE quantum dots,” The Journal of Physical Chemistry C, vol. 113, no. 45, pp. 19468–19474, Oct. 2009, doi: 10.1021/jp906827m.
[54] Safari, S. Matloub, and M. J. Connelly, “Accelerating gain and phase recovery in Quantum-Dot reflective Semiconductor optical Amplifier: Unraveling the influence of inhomogeneous broadening and pumping power for enhanced performance,” Optics & Laser Technology, vol. 182, p. 112089, Nov. 2024, doi: 10.1016/j.optlastec.2024.112089.
[55] Henini, “Quantum Dot Heterostructures; D. Bimberg, M. Grundmann, N.N. Ledenstov; Wiley, New York, ISBN 0 471 97388 2, £90,” Microelectronics Journal, vol. 31, no. 2, pp. 148–149, Feb. 2000, doi: 10.1016/s0026-2692(99)00093-2.
[56] Shen et al., “Low confinement factor quantum dash (QD) mode-locked Fabry-Perot (FP) laser diode for tunable pulse generation,” OFC/NFOEC 2008 - 2008 Conference on Optical Fiber Communication/National Fiber Optic Engineers Conference, pp. 1–3, Feb. 2008, doi: 10.1109/ofc.2008.4528481.
[57] H. Dortaj, M. Faraji, and S. Matloub, “High-speed and high-contrast two-channel all-optical modulator based on solution-processed CdSe/ZnS quantum dots,” Scientific Reports, vol. 12, no. 1, Jul. 2022, doi: 10.1038/s41598-022-17084-4.
[58] Hadi, B., Shama, F., Sherafat Vaziri, H., Eghbalkhah, M. (2024). 'A Piezoresistive Pressure Sensor Modeling by Artificial Neural Networks', Journal of Optoelectronical Nanostructures, 9(4), pp. -. doi: 10.30495/jopn.2024.32877.1308
[59] Soleimiani, M., Karimi, M. J., Rahimi, H. (2024). 'Light absorption and short-circuit current density in plasmonic organic solar cells containing liquid crystal and metal nanowires', Journal of Optoelectronical Nanostructures, 9(4), pp. -. doi: 10.30495/jopn.2024.33665.1325
[60] Mehrpanah, A., Rasooli Saghai, H., Sakkaki, B., Daghigh, A. (2024). 'Absorption Enhancement of Thin Film Solar Cell Utilizing a Graphene-Based Metasurface', Journal of Optoelectronical Nanostructures, 9(4), pp. -. doi: 10.30495/jopn.2024.33743.1330

[61] Haddadan, F., Soroosh, M., Singh, J. (2024). 'Designing an electro-optical 8-to-3 encoder based on resonant cavity and graphene-Al2O3 stack in the photonic crystal platform', Journal of Optoelectronical Nanostructures, 9(4), pp. -. doi: 10.30495/jopn.2024.33689.1328
[62] Mirkamali, A., khalimovich Muminov, K. , Numerical Simulation of CdS/CIGS Tandem Multi-Junction Solar Cells with AMPS-1D, Journal of Optoelectronical Nanostructures, 2(1), 31-40 ,2017.